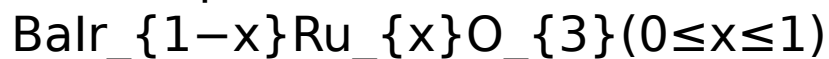




CHORUS

This is the accepted manuscript made available via CHORUS. The article has been published as:

Ground-state tuning of metal-insulator transition by compositional variations in



S. J. Yuan, K. Butrouna, J. Terzic, H. Zheng, S. Aswartham, L. E. DeLong, Feng Ye, P. Schlottmann, and G. Cao

Phys. Rev. B **93**, 165136 — Published 25 April 2016

DOI: [10.1103/PhysRevB.93.165136](https://doi.org/10.1103/PhysRevB.93.165136)

**Ground state tuning of the metal-insulator transition by
compositional variations in $\text{BaIr}_{1-x}\text{Ru}_x\text{O}_3$ ($0 \leq x \leq 1$)**

S. J. Yuan^{1*}, K. Butrouna¹, J. Terzic¹, H. Zheng¹, S. Aswartham¹, L. E. DeLong¹,
Feng Ye², P. Schlottmann³ and G. Cao^{1*}

¹ Center for Advanced Materials and Department of Physics and Astronomy, University of
Kentucky, Lexington, Kentucky 40506, USA

² Quantum Condensed Matter Division, Oak Ridge National Laboratory,
Oak Ridge, Tennessee 37831, USA

³ Department of Physics, Florida State University, Tallahassee, FL 32306, USA

ABSTRACT

Hexagonal BaIrO_3 is a magnetic insulator driven by the spin-orbit interaction (SOI), whereas BaRuO_3 is an enhanced paramagnetic metal. Our investigation of structural, magnetic, transport and thermal properties reveals that substitution of Ru^{4+} ($4d^4$) ions for Ir^{4+} ($5d^5$) ions in BaIrO_3 reduces the magnitudes of the SOI and a monoclinic structural distortion, and rebalances the competition between the SOI and the lattice degrees of freedom to render an evolution from a magnetic insulating state to a robust metallic state. The central findings of this work are (1) light Ru doping ($0 < x \leq 0.15$) prompts simultaneous, precipitous drops in both the magnetic ordering temperature T_N and the electrical resistivity, and (2) heavier Ru doping ($0.41 \leq x \leq 0.9$) induces a robust metallic state without any long-range magnetic order. All results suggest a critical role of the lattice degrees of freedom in determining the ground state in the heavy transition metal oxides.

PACS numbers: 71.70.Ej, 75.30.Gw, 71.30.+h

I. INTRODUCTION

A unique feature of the 5d-iridates is that a strong spin-orbit interaction (SOI) competes vigorously with Coulomb interactions, non-cubic crystalline electric fields, and Hund's rule coupling[1-5]. The relative strengths of these interactions stabilize new exotic ground states that provide a fertile ground for studying new physics. In particular, it is now recognized that strong SOI can drive novel, narrow-gap Mott insulating states in iridates. The SOI is a relativistic effect that is proportional to Z^2 (Z is the atomic number), and is approximately 0.4 eV in the iridates (compared to ~ 20 meV in 3d materials), and splits the t_{2g} bands into states with $J_{\text{eff}} = 1/2$ and $J_{\text{eff}} = 3/2$, the latter having lower energy. Since the Ir^{4+} ($5d^5$) ions provide five 5d valence electrons, four of them fill the lower $J_{\text{eff}} = 3/2$ bands, and one electron partially occupies the $J_{\text{eff}} = 1/2$ band in which the Fermi level E_F resides. The $J_{\text{eff}} = 1/2$ band is so narrow that even a reduced U (~ 0.50 eV, due to the extended nature of 5d-electron orbitals) is sufficient to open a gap (≤ 0.62 eV) that induces a novel insulating state, which is contrary to expectations based upon the relatively large, unsplit 5d bandwidth[1-3,6].

Adopting a distorted hexagonal structure with both face-sharing and corner-sharing IrO_6 octahedra, BaIrO_3 is particularly unique, in that it exhibits a simultaneous onset of weak ferromagnetic transition due to a canted antiferromagnetic (AFM) structure and charge density wave (CDW) orders with Néel temperature $T_N = 183$ K, comparable to that of other iridates, such as 240 K for Sr_2IrO_4 [7] and 285 K for $\text{Sr}_3\text{Ir}_2\text{O}_7$ [8], and a temperature-driven transition from a bad-metal to an insulating ground state [9-11]. The ground state of BaIrO_3 is extremely sensitive to lattice contractions that can be tuned by light doping or the application of hydrostatic pressures [4,12,13]. The extraordinary delicacy of the ground state in BaIrO_3 implies a critical balance between orbital, electronic, and lattice degrees of freedom [4,14]. The hexagonal structure of BaIrO_3 is similar to that of nine-layered, rhombohedral BaRuO_3 , which exhibits a crossover from metallic to insulating behavior and enhanced paramagnetism with decreasing temperature [15,16]. However, a

monoclinic distortion extant in BaIrO₃ at room temperature and 90 K generates twisting and buckling of the cluster trimmers (see Fig. 1) that give rise to two one-dimensional (1D) zigzag chains along the *c*-axis, and a two-dimensional (2D) layer of corner-sharing IrO₆ octahedra in the *ab* plane [9,12,17-19].

Although BaIrO₃ and BaRuO₃ have similar structures, they exhibit sharply contrasting physical properties, which underscores the critical role SOI (~0.4 eV for iridates, and ~0.15 eV for ruthenates)[3] and the lattice degrees of freedom can play in determining the ground state in iridates. In this work, substituting Ru⁴⁺ (*4d*⁴) for Ir⁴⁺ (*5d*⁵) in single-crystal BaIr_{1-x}Ru_xO₃ ($0 \leq x \leq 1$) reduces the magnitude of the SOI, the structural distortions and adds holes to the *t*_{2g} bands. The overall effect of Ru doping is to lower *E*_F and move the system away from the Mott instability toward a more robust metallic state. The emerging metallic state with delocalized electrons also accompanies a decrease in T_N.

II. EXPERIMENTAL

The single crystals of BaIr_{1-x}Ru_xO₃ were grown by conventional flux methods similar to earlier reports [9,15], using BaCl₂ as self-flux. Crystals were grown in platinum crucibles using IrO₂ (99.98%, Alfa Aesar), RuO₂ (99.98%, Alfa Aesar), BaCO₃ (99.99%, Alfa Aesar) and anhydrous BaCl₂ (99.5%, Alfa Aesar). Starting powders were placed in a Pt crucible with a Pt lid, and this assembly was then put in an alumina crucible with a cover. The mixtures were heated up to 1480 °C, and then cooled to 1350 °C at a rate of 5 °C per hour, before cooling down to room temperature. The ratio of the sample to flux remains at 1:8 throughout the entire series of BaIr_{1-x}Ru_xO₃. The crystals have a hexagonal surface and a visible layered texture along the *c*-axis, as shown in the inset of Fig. 2(a). The crystal structures were determined using a Nonius Kappa CCD X-ray diffractometer or a Rigaku X-ray diffractometer XtaLAB PRO equipped with PILATUS 200K hybrid pixel array detector at 90 K or 240 K, and they were refined by full-matrix, least squares using the SHELX-97 programs [20]. The standard deviations of all lattice parameters and interatomic distances are smaller than 0.1%. The atomic parameters for BaIr_{1-x}Ru_xO₃

are available in Supplemental Material (SM)[21]. Chemical compositions of the single crystals were estimated using a combined unit of Hitachi/Oxford SwiftED 3000 for energy dispersive X-ray (EDX) spectroscopy. The magnetization $M(T)$, electrical resistivity $\rho(T)$ and specific heat $C(T)$ were measured between 1.7 K and 400 K using a Quantum Design 7T SQUID Magnetometer and a Quantum Design 9T Physical Property Measurement System, respectively.

III. RESULTS AND DISCUSSION

The two end members BaIrO_3 and BaRuO_3 both have 9 layers rhombohedral phase with different space groups, as shown in Fig. 1(a)&(b). The $C2/m(12)$ space group of BaIrO_3 features three face-sharing IrO_6 octahedra forming Ir_3O_{12} trimers that are corner- and face-shared via IrO_6 octahedra (containing Ir1 and Ir3 sites) to form one-dimensional (1D) chains along the c -axis [12,16-19] (see Fig. 1(a)). A monoclinic distortion generates twisting and buckling of the trimers (tilted $\sim 12^\circ$ relative to each other), which gives rise to two 1D zigzag chains along the c -axis, and a two-dimensional layer of corner-sharing IrO_6 octahedra in the ab -plane. Substituting Ru^{4+} for Ir^{4+} preserves the monoclinic structure in the entire doping range ($x \leq 0.90$) except for $x = 1$, as shown in Table 1. It results in a nearly uniform reduction in lattice parameters a , b and c axes, and the unit cell volume V . This behavior is expected because the ionic radius of Ru^{4+} (0.620 Å) is slightly smaller than that of Ir^{4+} (0.625 Å). In addition, the Ir/Ru-O-Ir/Ru bond angle θ increases linearly with increasing Ru concentration x and eventually reaches 180° for $x = 1$ (i.e., BaRuO_3), indicating a significantly less distorted lattice. BaRuO_3 or $x=1$ exhibits a similar crystal structure with the $R\bar{3}m(166)$ space group, as shown in Fig. 1(b). Three RuO_6 octahedra share faces in a partial chain, facilitating direct Ru-Ru d -orbital interactions between the octahedra. Each of these triple units or trimmers of octahedra shares corners with its neighbors along the hexagonal axis via nearly 180° bonds angle that favor superexchange coupling (Fig.1(b)).

Ru doping induces pronounced changes in a wide range of physical properties of

single-crystal $\text{BaIr}_{1-x}\text{Ru}_x\text{O}_3$. Representative data for the c -axis magnetic susceptibility $\chi_c(T)$ that shows the weak magnetic transition at T_N is depressed from 183 K for $x = 0$, to 145 K for $x = 0.04$, and vanishes for $x \geq 0.41$, as shown in Fig. 2.

The magnetic anisotropy also decreases with Ru additions, as shown in Fig. 3. Magnetic anisotropy is in general a result of SOI; Ru doping weakens the SOI, therefore, leading to a smaller magnetic anisotropy. Furthermore, the Hund's rule coupling competes with the SOI, thus weakens the relative strength of the SOI. With increasing x , the c -axis susceptibility $\chi_c(T)$ becomes relatively stronger and larger than the basal-plane susceptibility $\chi_{ab}(T)$ (see Fig. 3 (b) & (c)). This change suggests a spin-flop from the basal-plane to the c -axis due to Ru doping. For $x = 1$, the basal-plane $\chi_{ab}(T)$ is larger than $\chi_c(T)$ again (see Fig.3 (d)). Similar phenomena were also observed in $\text{Ca}_2\text{Ru}_{1-x}\text{Ir}_x\text{O}_4$ [22] and $\text{Sr}_2\text{Ir}_{1-x}\text{Ru}_x\text{O}_4$ [23]. This behavior could be due to the strong interaction between Ru 4d- and Ir 5d-electrons.

It is already established that the bond angle θ is critical to the electronic and magnetic structure of iridates [4]. As shown in Fig. 4(a), θ increases linearly with increasing x and eventually reaches an ideal 180° for $x = 1$. The increase in θ directly enhances the electron hopping and favors a more metallic state with a concurrent decrease in T_N (see Fig.4(b)).

Indeed, the evolution from the insulating to itinerant state upon Ru doping is clearly illustrated in the electrical resistivity $\rho(T)$. For $x = 0$, both the ab -plane and c -axis, $\rho_{ab}(T)$ and $\rho_c(T)$ exhibit a sharp kink at $T_N = 183$ K, consistent with previous results in which the energy gap is estimated to be 0.1 eV [9,17]. With Ru doping, both $\rho_{ab}(T)$ and $\rho_c(T)$ decrease rapidly (see Fig.5). It is noted that the metallic behavior at higher temperatures for $x = 0.04$ (see Fig.5(b)) does not seem to follow a general trend displayed by other compositions although the behavior is highly reproducible. The origin of this brief occurrence of the metallic state is yet to be understood. Nevertheless, dilute Ru substitutions for Ir result in a reduced $\rho(T)$ and an emerging metallic state for $x > 0.15$. For $x = 1$ or BaRuO_3 , a broad upturn in $\rho_{ab}(T)$ at low temperatures might be a result of a pseudogap formation and 1D-CDW fluctuations, according to Ref. [16].

The temperature dependence of the specific heat $C(T)$ for various x is given in Fig. 6(a). Fitting the data to $C(T) = \gamma T + \beta T^3$ for $7 < T < 17$ K yields the Sommerfeld coefficient γ for the electronic contribution to $C(T)$ (see Fig. 6(b)), which serves as a measure of the electronic density of states at the Fermi level, $N(E_F)$, and the effective mass of the carriers. There is a substantial increase of γ with dilute Ru concentration; in particular, γ reaches 11.75 mJ/mol K² for $x = 0.04$, and 15.09 mJ/mol K² for $x = 0.15$, compared to $\gamma = 2.34$ mJ/mol K² for the parent compound ($x = 0.0$). The γ for $0.04 \leq x \leq 0.15$, in which the metallic state is not fully developed, is unexpectedly high, and this is likely due to spin fluctuations existent in the system. Nevertheless, $N(E_F)$ and γ eventually decrease with x , as shown in Fig. 6(b). In the case of BaRuO₃, the smaller values reflect pseudogap formation due to the CDW instability [16].

IV. CONCLUSIONS

We have investigated the structural, magnetic, transport and thermal properties of BaIr_{1-x}Ru_xO₃. Ru doping rebalances the competition between the SOI, electron correlations and the lattice degrees of freedom to generate a metallic state for $x > 0.15$. The Ru doping alters the relative strength of the SOI that dictate the ground state, which, in turn, affects the band gap near E_F . Unlike the situation in Sr₂IrO₄ that features an unconventional correlation between the magnetic transition and charge gap, the evolution of the ground state in BaIr_{1-x}Ru_xO₃ appears to indicate a strong coupling between the magnetic order and metal-insulator transition. All results suggest a critical role of lattice degrees of freedom that along with the SOI dictates the ground state of the heavy transition metal oxides.

ACKNOWLEDGMENTS

This work was supported by the National Science Foundation via Grant No. DMR-1265162 (GC), Department of Energy (BES) through grants No. DE-FG02-98ER45707 (PS) and DE-FG02-97ER45653 (L.E.D.).

*Corresponding author: siyuan.shu@gmail.com, cao@uky.edu

REFERENCES

- [1] B. J. Kim, H. Jin, S. J. Moon, J. Y. Kim, B. G. Park, C. S. Leem, J. Yu, T. W. Noh, C. Kim, S. J. Oh, J. H. Park, V. Durairaj, G. Cao, and E. Rotenberg, *Physical Review Letters* **101**, 076402 (2008).
- [2] B. J. Kim, H. Ohsumi, T. Komesu, S. Sakai, T. Morita, H. Takagi, and T. Arima, *Science* **323**, 1329 (2009).
- [3] G. Cao and L. E. DeLong, in *Frontiers of 4d- and 5d-Transition Metal Oxides* (World Scientific, Singapore, 2013).
- [4] O. B. Korneta, S. Chikara, S. Parkin, L. E. DeLong, P. Schlottmann, and G. Cao, *Physical Review B* **81**, 045101 (2010).
- [5] T. F. Qi, O. B. Korneta, L. Li, K. Butrouna, V. S. Cao, X. Wan, P. Schlottmann, R. K. Kaul, and G. Cao, *Physical Review B* **86**, 125105 (2012).
- [6] J. Dai, E. Calleja, G. Cao, and K. McElroy, *Physical Review B* **90**, 041102 (2014).
- [7] G. Cao, J. Bolivar, S. McCall, J. E. Crow, and R. P. Guertin, *Physical Review B* **57**, R11039 (1998).
- [8] G. Cao, Y. Xin, C. S. Alexander, J. E. Crow, P. Schlottmann, M. K. Crawford, R. L. Harlow, and W. Marshall, *Physical Review B* **66**, 214412 (2002).
- [9] G. Cao, J. E. Crow, R. P. Guertin, P. F. Henning, C. C. Homes, M. Strongin, D. N. Basov, and E. Lochner, *Solid State Communications* **113**, 657 (2000).
- [10] M. L. Brooks, S. J. Blundell, T. Lancaster, W. Hayes, F. L. Pratt, P. P. C. Frampton, and P. D. Battle, *Physical Review B* **71**, 220411 (2005).
- [11] M. A. Laguna-Marco, D. Haskel, N. Souza-Neto, J. C. Lang, V. V. Krishnamurthy, S. Chikara, G. Cao, and M. van Veenendaal, *Physical Review Letters* **105**, 216407 (2010).
- [12] G. Cao, X. N. Lin, S. Chikara, V. Durairaj, and E. Elhami, *Physical Review B* **69**, 174418 (2004).
- [13] M. A. Laguna-Marco, G. Fabbris, N. M. Souza-Neto, S. Chikara, J. S. Schilling, G. Cao, and D. Haskel, *Physical Review B* **90**, 014419 (2014).
- [14] W. Ju, G.-Q. Liu, and Z. Yang, *Physical Review B* **87**, 075112 (2013).
- [15] M. Shepard, S. McCall, G. Cao, and J. E. Crow, *Journal of Applied Physics* **81**, 4978 (1997).
- [16] Y. S. Lee, J. S. Lee, K. W. Kim, T. W. Noh, J. Yu, Y. Bang, M. K. Lee, and C. B. Eom, *Physical Review B* **64**, 165109 (2001).
- [17] A. V. Powell and P. D. Battle, *Journal of Alloys and Compounds* **191**, 313 (1993).
- [18] M. H. Whangbo and H. J. Koo, *Solid State Communications* **118**, 491 (2001).
- [19] R. Lindsay, W. Strange, B. L. Chamberland, and R. O. Moyer Jr, *Solid State Communications* **86**, 759 (1993).
- [20] G. Sheldrick, *Acta Crystallographica Section A* **64**, 112 (2008).
- [21] See Supplemental Material at [URL will be inserted by publisher] for substantial information on crystal refinements.
- [22] S. J. Yuan, J. Terzic, J. C. Wang, L. Li, S. Aswartham, W. H. Song, F. Ye, and G. Cao, *Physical Review B* **92**, 024425 (2015).
- [23] S. J. Yuan, S. Aswartham, J. Terzic, H. Zheng, H. D. Zhao, P. Schlottmann, and G. Cao, *Physical Review B* **92**, 245103 (2015).

Figure Captions

FIG. 1. Comparison of the nine-layer crystallographic form (a) BaIrO₃ and (b) BaRuO₃ crystal structure. Note the corner-sharing Ir₃O₁₂ and Ru₃O₁₂ trimers that are connected through the vertices of the top and bottom octahedra of the trimers, and the schematic of the M–O₂–M bond angle θ (M = Ir or Ru).

FIG. 2. The magnetic susceptibilities $\chi(T)$ along c axis for BaIr_{1-x}Ru_xO₃, where (a) $0 \leq x \leq 0.15$ and (b) $0.42 \leq x \leq 1$. The data were collected after field cooling procedure at $\mu_0 H = 0.1$ T. The inset in (a) shows a representative single crystal of BaIr_{1-x}Ru_xO₃ with $x = 0$. The inset in (b) shows an enlarged $\chi_c(T)$ for $x = 0.15$.

FIG. 3. The magnetic susceptibilities $\chi(T)$ in ab plane and along c axis respectively for representative compositions (a) $x = 0$, (b) $x = 0.10$, (c) $x = 0.82$, and (d) $x = 1$. The magnetization was measured after field cooling at $\mu_0 H = 0.1$ T.

FIG. 4. The Ru concentration x dependence of (a) the Ir/Ru–O₂–Ir/Ru bond angle θ and (b) T_N . Inset: Schematic of the Ir/Ru–O₂–Ir/Ru bond angle θ . Note that θ increases linearly with increasing x .

FIG. 5. The temperature dependence of the resistivity $\rho(T)$ for representative compositions (a) $x = 0$, (b) $x = 0.04$, (c) $x = 0.15$, (d) $x = 0.41$, (e) $x = 0.63$, (f) $x = 0.82$, (g) $x = 0.90$ and (h) $x = 1$. The vertical arrows indicate the kink that corresponds to the weak magnetic transition at $T = T_N$.

FIG. 6. (a) The specific heat $C(T)/T$ vs T^2 , and (b) the Sommerfeld coefficient γ vs x , for BaIr_{1-x}Ru_xO₃.

Table 1. The crystal structure and refinement details of BaIr_{1-x}Ru_xO₃ at 90 K for x = 0, 0.10, 0.63 and 1, and at 240 K for x=0.82 and 0.90. The diffractometer is Nonius KappaCCD and the absorption correction is multi-scan SADABS. The Ir/Ru–O₂–Ir/Ru bond angle is defined in Fig.1.

	x = 0 (90K)	x = 0.10 (90K)	x = 0.63 (90K)	x = 0.82 (240K)	x = 0.90 (240K)	x = 1 (90K)
Crystal data						
Crystal system,	Monoclinic,	Monoclinic,	Monoclinic,	Monoclinic,	Monoclinic,	Trigonal,
space group	C12/m1(12)	C12/m1(12)	C12/m1(12)	C12/m1(12)	C12/m1(12)	$R\bar{3}m$ (166)
a,b,c (Å)	a=9.9935(2), b= 5.7352(1), c=15.2376(3)	a=9.9839(2), b=5.7377(1), c=15.1107(4)	a=9.9440(2), b=5.7429(1), c=14.8102(4)	a=9.9999(5), b=5.7759(4), c=14.8916(4)	a= 9.9923(4), b= 5.7733(3), c= 14.8882(8)	a=5.7366(1), c=21.5933(6)
β (°)	103.411(1)	103.3402(9)	102.8574(9)	102.939(5)	102.882(4)	NA
V (Å³)	849.10(6)	842.25(3)	824.57(3)	838.28(8)	837.26(7)	615.40(3)
Z	12	12	12	12	12	9
Bond angle (°)	161.671(1)	163.678(0)	174.296(1)	175.1(3)	176.1(1)	180.0
Data collection						
No. of measured, independent and observed [I>4σ(I)] reflections	6066, 398, 350	7075, 396, 369	7210,398, 353	14459,1643, 1525	14071,1769, 1633	7256,401, 398
Rint	0.021	0.031	0.035	0.027	0.038	0.025
Refinement						
R[F²>4σ(F²)],w	0.016, 0.035,	0.02, 0.049,	0.025, 0.069,	0.067, 0.1847,	0.072,0.205,	0.02, 0.035,
R(F²),S	1.05	1.15	1.17	1.085	1.024	1.09

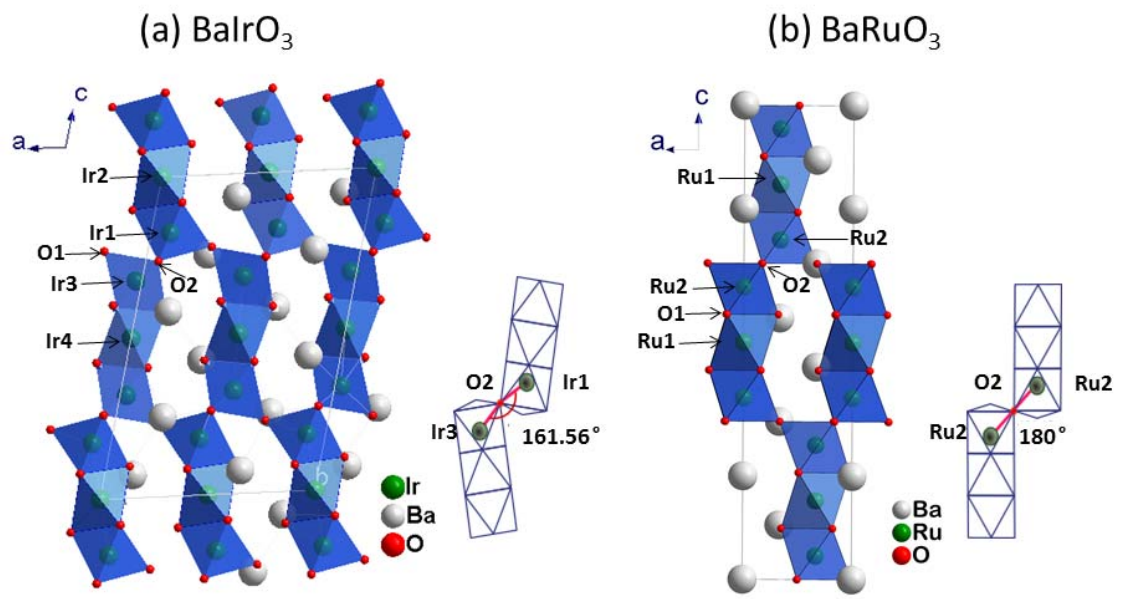


Fig.1

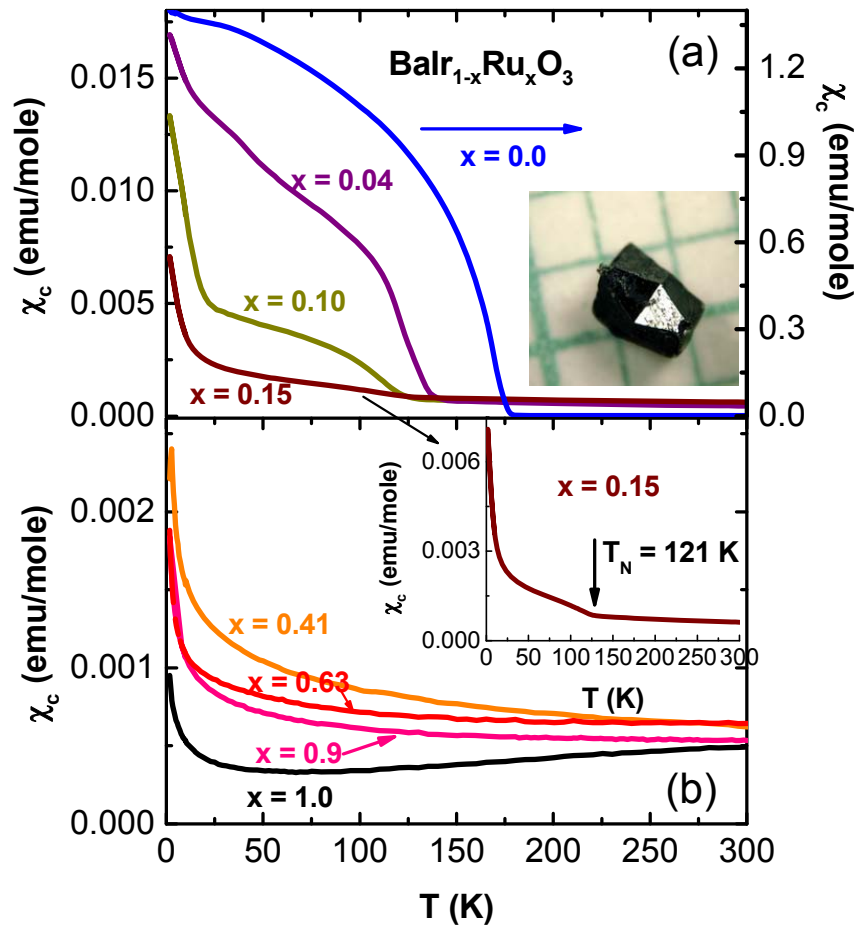


Fig.2

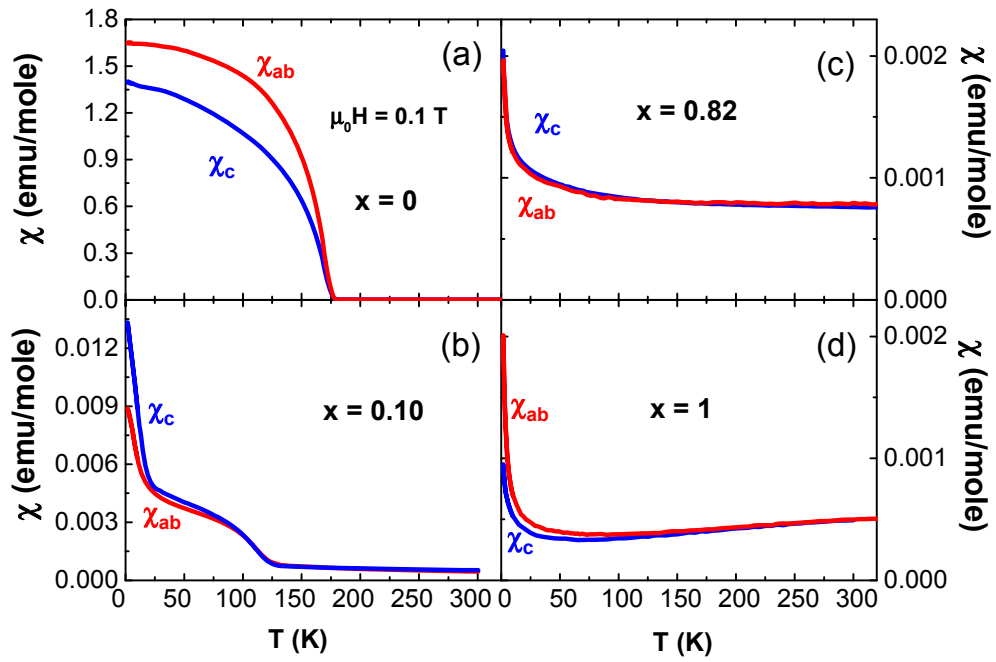


Fig.3

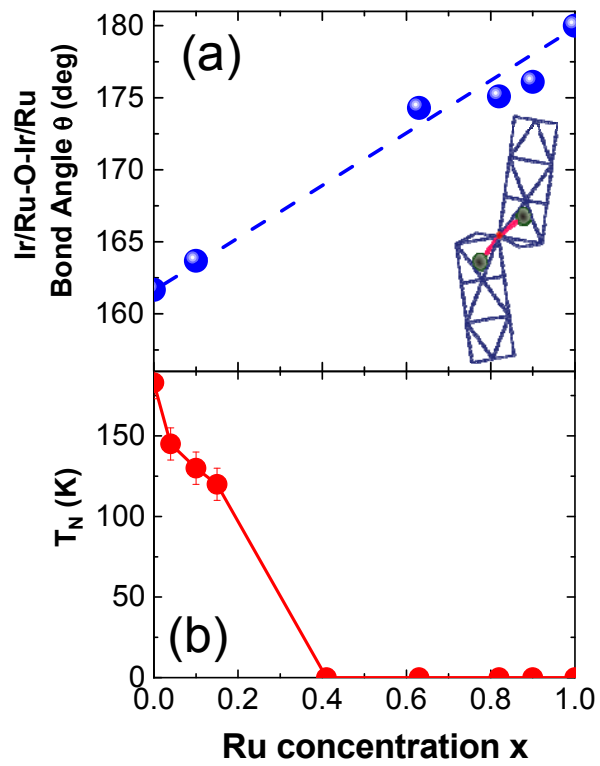


Fig. 4

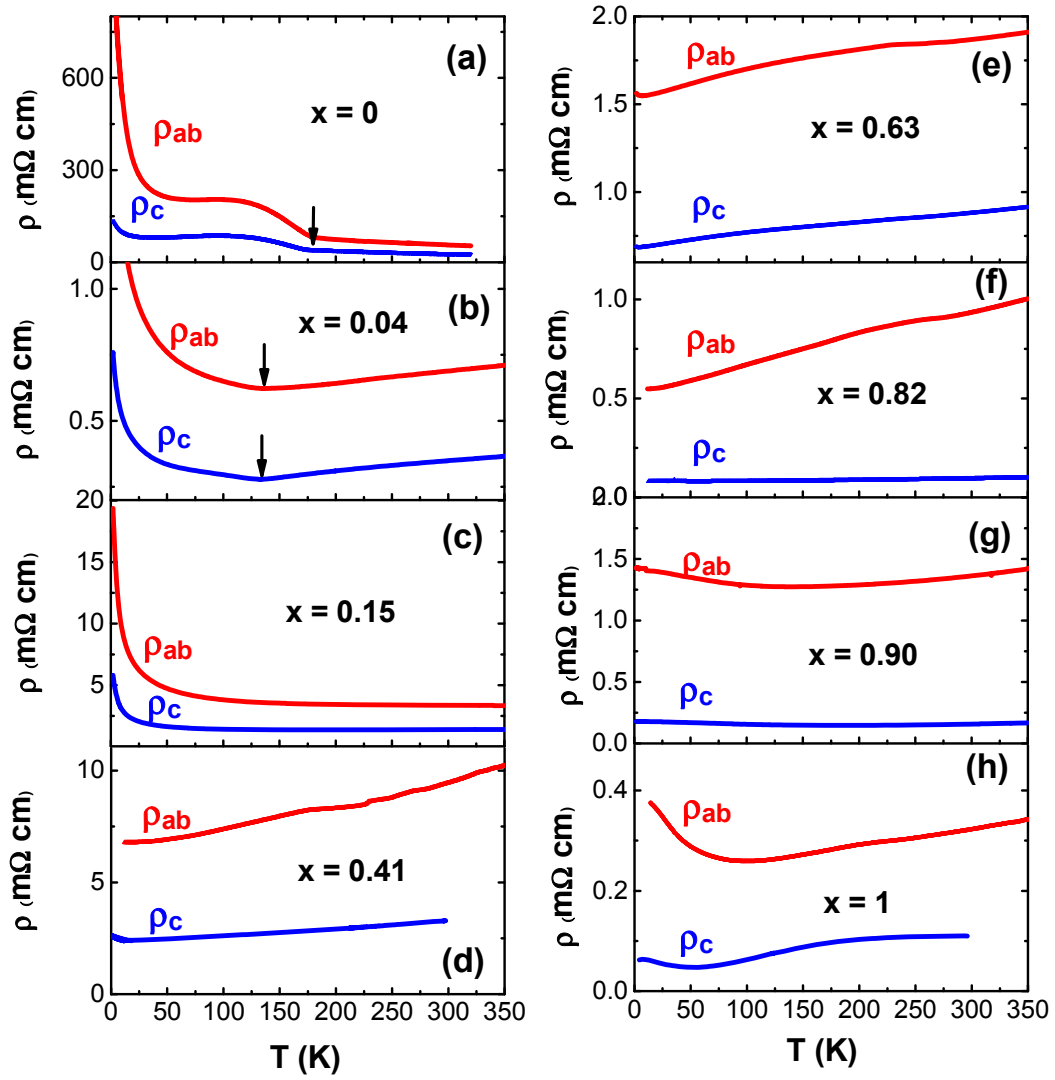


Fig.5

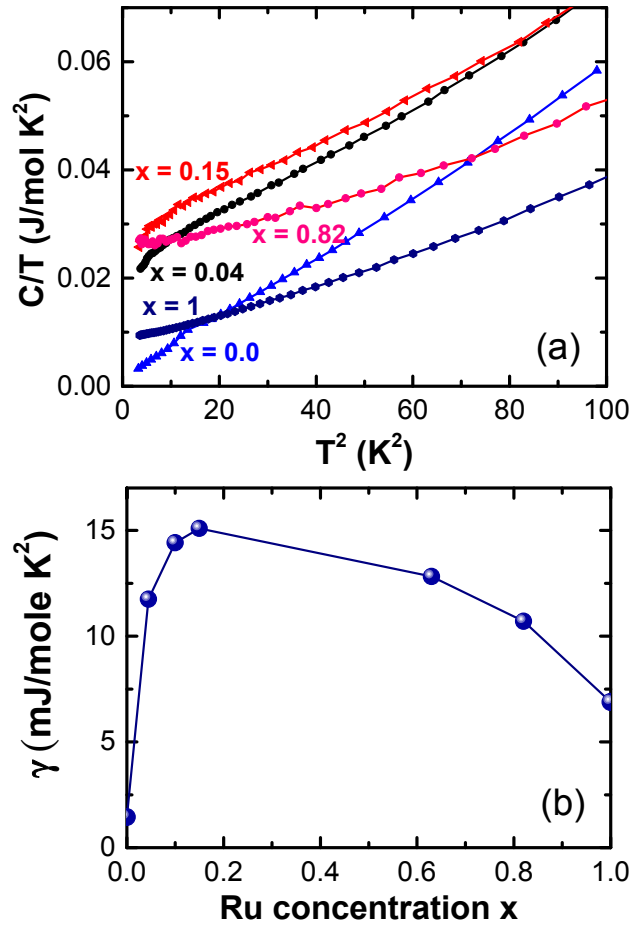


Fig.6